JCI The Journal of Clinical Investigation

The diabetogenic mouse MHC class II molecule I-A^{g7} is endowed with a switch that modulates TCR affinity

Kenji Yoshida, … , Ian A. Wilson, Luc Teyton

J Clin Invest. 2010;120(5):1578-1590. https://doi.org/10.1172/JCI41502.

Research Article

Genetic susceptibility to autoimmunity is frequently associated with specific MHC alleles. Diabetogenic MHC class II molecules, such as human HLA-DQ8 and mouse I-A^{g7}, typically have a small, uncharged amino acid residue at position 57 of their β chain (β57); this results in the absence of a salt bridge between β57 and Argα76, which is adjacent to the P9 pocket of the peptide-binding groove. However, the influence of Argα76 on the selection of the TCR repertoire remains unknown, particularly when the MHC molecule binds a peptide with a neutral amino acid residue at position P9. Here, we have shown that diabetogenic MHC class II molecules bound to a peptide with a neutral P9 residue primarily selected and expanded cells expressing TCRs bearing a negatively charged residue in the first segment of their complementarity determining region 3β. The crystal structure of one such TCR in complex with I-A^{g7} bound to a peptide containing a neutral P9 residue revealed that a network of favorable long-range (greater than 4 Å) electrostatic interactions existed among Argα76, the neutral P9 residue, and TCR, which supported the substantially increased TCR/peptide-MHC affinity. This network could be modulated or switched to a lower affinity interaction by the introduction of a negative charge at position P9 of the peptide. Our results support the existence of a switch at residue β57 […]

The diabetogenic mouse MHC class II molecule I-A^{g7} is endowed with a switch that modulates TCR affinity

Kenji Yoshida,[1] Adam L. Corper,[2] Rana Herro,[1] Bana Jabri,[3] Ian A. Wilson,[2,4] and Luc Teyton[1]

[1]Department of Immunology and Microbial Science, and [2]Department of Molecular Biology, The Scripps Research Institute, La Jolla, California, USA. [3]University of Chicago, Department of Medicine and Committee on Immunology, Chicago, Illinois, USA. [4]Skaggs Institute for Chemical Biology, The Scripps Research Institute, La Jolla, California, USA.

Genetic susceptibility to autoimmunity is frequently associated with specific MHC alleles. Diabetogenic MHC class II molecules, such as human HLA-DQ8 and mouse I-A^{g7}, typically have a small, uncharged amino acid residue at position 57 of their β chain (β57); this results in the absence of a salt bridge between β57 and Argα76, which is adjacent to the P9 pocket of the peptide-binding groove. However, the influence of Argα76 on the selection of the TCR repertoire remains unknown, particularly when the MHC molecule binds a peptide with a neutral amino acid residue at position P9. Here, we have shown that diabetogenic MHC class II molecules bound to a peptide with a neutral P9 residue primarily selected and expanded cells expressing TCRs bearing a negatively charged residue in the first segment of their complementarity determining region 3β. The crystal structure of one such TCR in complex with I-A^{g7} bound to a peptide containing a neutral P9 residue revealed that a network of favorable long-range (greater than 4 Å) electrostatic interactions existed among Argα76, the neutral P9 residue, and TCR, which supported the substantially increased TCR/peptide-MHC affinity. This network could be modulated or switched to a lower affinity interaction by the introduction of a negative charge at position P9 of the peptide. Our results support the existence of a switch at residue β57 of the I-A^{g7} and HLA-DQ8 class II molecules and potentially link normal thymic TCR selection with abnormal peripheral behavior.

Introduction

An association between the HLA locus and autoimmune dysfunction was suggested as early as 1971 (1). Later, attention focused on MHC class II genes with the discovery of an association between HLA-DR4 and rheumatoid arthritis in 1978 (2). Thirty years have now passed since these seminal studies, and yet our general understanding of antigen presentation and T cell recognition at a molecular level has not provided an expected explanation for this association. One of the most striking examples of MHC allele linkage disequilibrium with autoimmune diseases is provided by type I diabetes (T1D) and the identification of a single residue polymorphism that confers either susceptibility or resistance to the disease (3). Indeed, almost all alleles linked to T1D share a common nonaspartic acid residue at position 57 of their β chain (3). The absence of a negative charge at β57 eliminates an interdomain salt bridge between Argα76 and β57; however, this substitution does not compromise the overall stability of the molecule or its capacity to bind peptide (4, 5). The absence of a negative charge at β57 reshapes the P9 pocket of the HLA-DQ8/I-A^{g7} peptide-binding groove and exposes a large positively charged patch on the MHC surface (4, 6). An important functional consequence of this β57 polymorphism is a clear propensity for these MHC molecules to bind peptides with a negatively charged residue at position P9. However, this feature is not absolute and many noncharged P9 peptides efficiently bind diabetogenic MHC molecules, such as HLA-DQ8 (7) or I-A^{g7} (5). These peptide-MHC (pMHC) complexes will as a result characteristically have an exposed positive P9 patch on the MHC surface due to the "unpaired" charged Argα76 residue.

We have investigated whether T cells could recognize this patch on such pMHC complexes. However, this region, and in particular β57, lies at the extreme end of the MHC peptide-binding groove and is typically beyond the reach (>10 Å) of the closest TCR loops (i.e., CDR2α and CDR3β). Hence, direct recognition of this part of pMHC might require the TCR to shift toward the C-terminal part of the peptide, away from its most common P5-centric position (8, 9). Our studies here were aimed at addressing this outstanding question and examining whether I-A^{g7}/HLA-DQ8 molecules could potentially support a unique mode of TCR recognition. Indeed, we have recently shown in celiac disease that the HLA-DQ8 β57 polymorphism promoted the recruitment of T cells bearing a negative charge in CDR3β during the response against native gluten peptides containing a neutral residue at P9, supporting the idea that this MHC polymorphism was directly affecting T cell responses (10). First, we expanded this observation to new antigenic systems and I-A^{g7}, and then we proceeded with structural and biophysical studies to discover potential mechanisms.

Results

Endogenous self peptides with non Asp/Glu P9 residue bias TCR CDR3β usage. We first determined whether our observation in the human HLA-DQ8/gliadin system (10) could be generalized to murine I-A^{g7} and other antigens by immunizing NOD mice with a glutamic acid decarboxylase 65 peptide (GAD) having a glycine (underlined) at P9 (LKKMREIIGWP<u>G</u>GSG; region 221–235 and hereafter designated GAD$_{221-235}$) or its variant GAD$_{221-235}$9E with a Glu at P9. Peptide-specific T cell hybridomas that were isolated and sequenced after

Authorship note: Kenji Yoshida and Adam L. Corper contributed equally to this work.

Conflict of interest: The authors have declared that no conflict of interest exists.

Citation for this article: *J Clin Invest.* 2010;120(5):1578–1590. doi:10.1172/JCI41502.

Table 1
Percentage of T cells carrying D/E residues in CDR3β segments

Antigen	P9 residue	% of CDR3β D/E	*P* value
$GAD_{221–235}$	G	69.2	0.019
$GAD_{221–235}$9E	E	18.2	
2.5mi P9G	G	51.6	0.047
2.5mi P9D	D	21.7	
$HEL_{11–27}$	G	68.0	0.246
$HEL_{11–27}$9E	E	50.0	
Total $CD4^+$ T cells	NA	22-30	N/A

TCR produced after immunization ($GAD_{221–235}$ and $HEL_{11–27}$) or from naive populations (2.5mi and total CD4). Sequencing was carried out on hybridomas (GAD), bulk-sorted $CD4^+$ T cells (total CD4; purity > 95%), or on single-sorted cells (tetramer sorting, 2.5mi and $HEL_{11–27}$). *P* values were calculated by Fisher's exact test. The amino acid sequences after CTC in TRBV1, LCG in TRBV20, CAW in TRBV31, or CAS in all other TRBVs and before YF, FF, TF, or LF in TRBJs were defined as CDR3β. The N-terminal region of CDR3β was defined as the first half of CDR3β.

RT-PCR cloning showed no bias in Vα or Vβ sequence usage for CDR1 or CDR2. However, most anti-I-$A^{g7}GAD_{221–235}$ T cell hybridomas carried a negative charge at positions 2 or 3 of their CDR3β (9/13, 69%) in contrast to T cells specific for $GAD_{221–235}$9E where no such bias was seen (2/11, 18%; Table 1 and Supplemental Tables 1 and 2; supplemental material available online with this article; doi:10.1172/JCI41502DS1).

We followed this result up in the context of another natural autoantigen and examined the BDC 2.5-like T cell response in NOD mice by sorting and analyzing single cells with I-A^{g7} tetramers displaying BDC 2.5 peptide mimotopes (11, 12) with either a negative charge (HHPIWARMDA; hereafter referred to as 2.5mi) or no charge at P9 (G or Q, named P9G and P9Q thereafter, HHPIWARMG/QA). The sequencing of individual TCR segments revealed an increase of negative residues in the CDR3β N-terminal region from cells sorted with P9Q or P9G tetramers (16/31, 52%) as compared with cells sorted with P9D tetramers (5/23, 21%; Table 1 and Supplemental Table 3). The latter frequency was comparable to the normal frequency of negative charges found in all purified $CD4^+$ CDR3β sequences in NOD mice (Table 1). The negative charges found in the CDR3β of the P9Q and P9G populations were encoded by N additions or deletions, suggesting an antigen-driven process (Supplemental Tables 3 and 4). This belief was also supported by the fact that P9G or P9Q tetramer–positive cells were found in higher numbers in the periphery than in the thymus and that over time, the population expanded early (3–4 weeks), then contracted (6–12 weeks) to reexpand later, especially in diabetic animals (Figure 1, A and B). In addition, the BDC 2.5 9Q/9G reactive TCR populations were found, up until week twelve, to be larger than the corresponding BDC 2.5 9D populations.

We next carried out FACS on polyclonal TCR populations (obtained from NOD mice) enriched by selection against I-A^{g7} 2.5mi 9Q or 9D tetramers (Figure 1C). The FACS profiles of these populations revealed that the mean fluorescence intensity of the $9Q^+$ reactive T cell population was significantly higher than $9D^+$, suggesting that the former were of higher affinity. The small size of these 2.5mi reactive T cell populations prevented us from carrying out tetramer decay experiments in order to estimate their respective avidities. We therefore carried out a depletion experiment whereby T cells reactive against I-A^{g7} 2.5mi 9Q tetramers were first depleted from the population. The flowthrough from this step was then stained against I-A^{g7} 2.5mi 9D tetramers, i.e., only T cells exclusively reactive against 2.5mi 9D were now identified (Figure 1C). Likewise, the reciprocal depletion experiment, i.e., deplete and select against I-A^{g7} 2.5mi 9D and 9Q, respectively, allowed us to identify T cells exclusively reactive against I-A^{g7} 2.5mi 9Q (Figure 1C). These experiments revealed that 3 distinct TCR populations exist in NOD mice: (a) TCRs reactive only to 2.5mi 9D, (b) TCRs that are reactive against either 2.5mi 9D or 9Q, and (c) TCRs that only react to 2.5mi 9Q. The latter TCR population is significantly higher than the "2.5mi 9D only" TCR population and also has a higher average affinity for pMHC as inferred by the higher mean fluorescence intensity.

In summary, these results suggested that a compensating mechanism existed where I-A^{g7} bound peptides with a neutral residue at position P9 were able to elicit TCRs with Asp/Glu residues (i.e., negatively charged) in the first segment of their CDR3β loop. Further, TCRs specific for the 2.5mi 9Q peptide have on average a higher avidity compared with TCRs raised against 2.5mi 9D.

Exogenous peptides with non-Asp/Glu P9 residues also bias TCR CDR3β usage. We then examined the TCR response against the classical exogenous antigen hen egg lysozyme (HEL) and its immunodominant $HEL_{11–27}$ peptide (AMKRHGLDNYRGYSLGN), which carries a Gly residue (underlined) at position P9. NOD mice were immunized with the peptide, and individual T cells were sorted after tetramer staining and analyzed by single-cell RT-PCR/sequencing to examine their CDR3β sequences. An increased number of negatively charged residues were found within the first 3 residues of the CDR3β loop for $CD4^+$ T cells specific against $HEL_{11–27}$ peptide (17/25, 68%; Table 1 and Supplemental Tables 5 and 6). The complementary immunization with a mutant peptide carrying a negative charge at P9 ($HEL_{11–27}$9E) and sorting of T cells with the same pMHC resulted in a lower percentage of TCRs carrying negatively charged residues in CDR3β (11/22, 50%; Table 1 and Supplemental Tables 5 and 6).

The results from those 3 different antigenic systems indicated that TCR recognition of I-A^{g7} peptide complexes was strongly associated with selection of a negatively charged residue in CDR3β when the peptide lacked an Asp/Glu at P9. This situation was identical to the one described for recognition of native gliadin peptide in the context of HLA-DQ8 (10), suggesting that TCR recognition of both HLA-DQ8 and I-A^{g7} was directly influenced by the nature of the P9 region.

Structure of I-$A^{g7}GAD_{221–235}$ suggests that the P9 pocket is accessible to TCR. A possible explanation for these observations was provided from our determination of the crystal structure of I-A^{g7} in complex with $GAD_{221–235}$ to 3.1 Å resolution (Supplemental Table 7). The packing of I-A^{g7}-$GAD_{221–235}$ within the crystal lattice revealed a striking feature, namely an I-A^{g7} dimer whose principal interface contact was formed as the direct result of the insertion of a glutamate side chain into the P9 peptide-binding pocket of another I-A^{g7} molecule (Figure 2A). This complementation of charge, although nonphysiological, confirmed that the positive patch created around P9 was surface accessible and hence could conceivably be directly recognized by the side chain of a negatively charged residue from a TCR.

A comparison of the electrostatic surfaces of I-$A^{g7}GAD_{221–235}$ and I-$A^{g7}GAD_{221–235}$9E (Figure 2B; the last structure was modeled from I-$A^{g7}GAD_{221–235}$) clearly showed that the I-$A^{g7}GAD_{221–235}$ surface was noticeably more positively charged around the P9 region

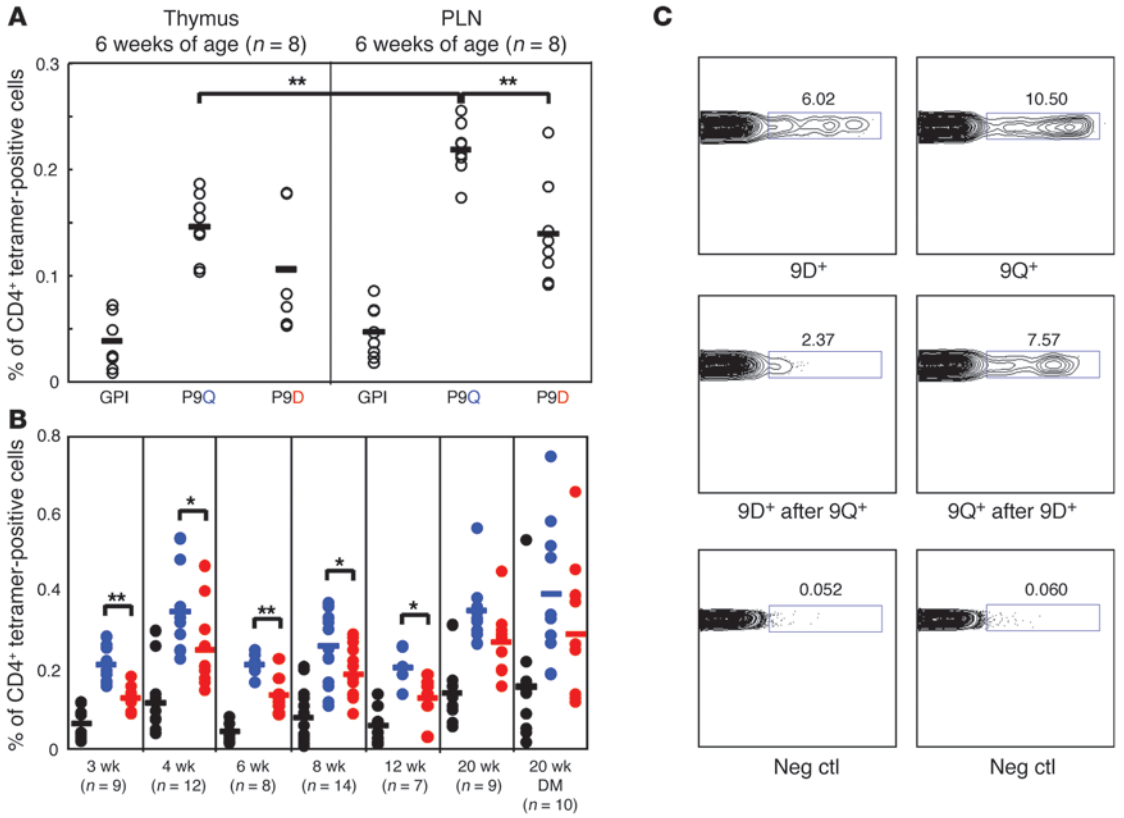

Figure 1

In vivo expansion of 2.5mi reactive T cells against either a negatively charged P9 peptide (Asp) or a neutral P9 peptide (Gln). (**A**) Both tetramer+ cell populations are present in the thymus and expand in the periphery (pancreatic lymph nodes [PLN]). I-A^{g7}GPI$_{282–292}$ was used as a negative control. Individual data points show the percentage of tetramer-positive cells for 1 mouse. (**B**) Modulation of the 2 populations over time in the pancreatic lymph nodes. DM indicates diabetic mice. *P < 0.05; **P < 0.01. Color scheme: black, I-A^{g7}GPI$_{282–292}$; blue, I-A^{g7} 2.5 mi 9Q; red, I-A^{g7} 2.5mi 9D. (**C**) 2.5mi T cell–reactive populations purified from 6-week-old NOD female mice spleens using I-A^{g7} 2.5mi 9D or 9Q tetramers and enriched with anti-PE beads on an autoMACS machine (top panel). The same experiment after first depleting either the 9D or 9Q T cell–reactive population (middle panel). Negative controls are CD4+ tetramer–negative cells (bottom panel). Displayed percentages are relative to the sorted CD4+ population.

due primarily to the presence of the uncompensated charge on the MHC residue Argα76. For I-A^{g7}GAD$_{221–235}$9E, the pairing of 9E with Argα76 resulted in the neutralization of the aforementioned unpaired positive charge. Importantly, the C terminus of the GAD$_{221–235}$ peptide does not contain any positively charged residues. Hence, the observed bias in the TCR CDR3β repertoire, seen between I-A^{g7}GAD$_{221–235}$ and I-A^{g7}GAD$_{221–235}$9E, cannot be attributed to the presence of a positively charged residue on the peptide itself. Thus, the enhanced presence of negatively charged residues in CDR3β for TCRs selected against I-A^{g7}GAD$_{221–235}$ is most likely linked to the introduction of favorable electrostatic interactions between TCR and the P9 region of I-A^{g7}.

An important question that remained unanswered at this point was whether the TCRs could be making direct contact with the P9 peptide side chain. If true, this would provide a simple explanation for our observations (i.e., skewing of the TCR repertoire). This mode of TCR binding would be surprising, since the P9 side chain is not easily accessible for TCR recognition, being positioned obliquely downwards and lying at the outermost edge of the TCR footprint. We surmised that the P9 side chain was unlikely to be directly involved in TCR recognition and concluded that this observation could only be explained by either direct recognition of the positively charged patch on the surface of I-A^{g7} or by an indirect effect (e.g., long-range electrostatic) that is secondary to the non-complementation of charge by the peptide at P9. The former possibility might require an important shift of the TCR footprint over MHC in order to place CDR3β over β57 (more than 10 Å). This mode of recognition could conceivably lead to a refocusing of the TCR CDR3 loops away from their normal P5-centric position.

Polyclonal TCR recognition of 2.5mi/HEL$_{11–27}$ is still P5 centric. The central role of the peptide P5 side chain for recognition by T cells was tested directly in the 2.5mi and HEL$_{11–27}$ systems by immunizing NOD mice with these peptides followed by in vitro stimulation of the responding CD4+ cells either with the eliciting peptide or a peptide variant with a glycine at position P5. In both cases, loss of a side chain at P5 resulted in no T cell activation (Supplemental Figure 1). This observation suggested that no major shift of the TCR along the MHC had occurred, although recognition of P5 by CDR1α (or CDR3α) could not be entirely discounted even following a shift of the TCR footprint.

In the absence of a TCR-pMHC structure, an explanation for this effect at a distance, other than electrostatic, was not easy to provide, but the functional consequences of a negative charge at P9 could be evaluated in the HEL system. Mice were immu-

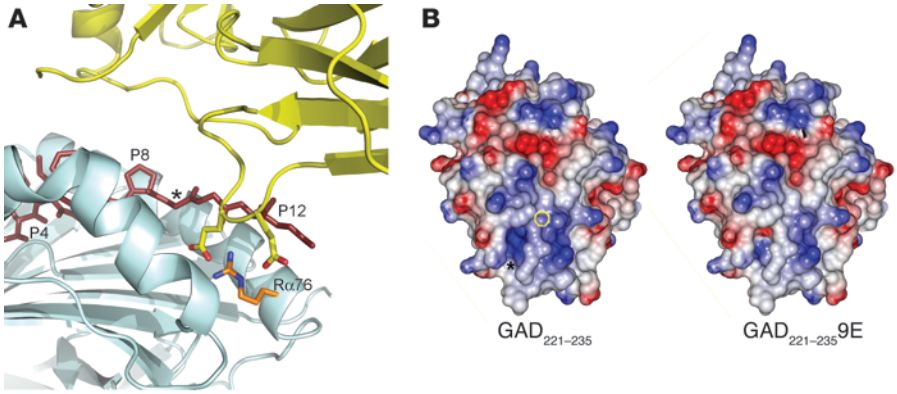

Figure 2
Analysis of the I-A^{g7}GAD$_{221–235}$ structure. (**A**) A nonphysiological I-A^{g7}GAD$_{221–235}$ dimer observed in the crystal. The principal interface contact is formed when the glutamate side chain (E$_{\alpha 171}$) of 1 MHC molecule binds in the P9 pocket of a second I-A^{g7} molecule in the crystal lattice. View is centered on the P9 pocket of I-A^{g7} (ribbon trace in cyan). The GAD peptide is displayed in ball-and-stick and appears as maroon. A symmetry-related I-A^{g7} is displayed as a ribbon trace in yellow. The GAD P9 peptide residue (Gly) is highlighted by an asterisk. (**B**) Electrostatic surfaces of I-A^{g7}GAD$_{221–235}$ (left) and I-A^{g7}GAD$_{221–235}$9E (right). The GAD$_{221–235}$ molecular surface is more positively charged around the P9 region (highlighted by an asterisk) compared with GAD$_{221–235}$9E. Positive charge is contoured blue, while negative charge is red (–5 to +5 kT/e). View is looking down onto the pMHC surface, with the P9 peptide residue circled.

nized with either WT HEL$_{11–27}$ peptide or HEL$_{11–27}$9E peptide and tested for proliferation in vitro (Figure 3). In all experiments (n = 4), the in vitro recall response with the HEL$_{11–27}$ peptide was always superior to the response to the mutant 9E peptide (Figure 3A), whereas in the reciprocal situation (immunization with 9E), both responses were equivalent (Figure 3B). These results indicated that the chemical nature of the P9 residue was a critical factor for the amplitude of the resulting polyclonal response and could influence the activation of a CD4 population selected with a peptide with Gly at P9.

Representative T cell hybridomas were isolated after HEL$_{11–27}$ or HEL$_{11–27}$9E immunizations (clones 21.30.7 and 72.10, respectively) and tested for activation by HEL$_{11–27}$ and mutant peptides. Clone 21.30.7 (hereafter called 21.30) was, analogous to the polyclonal response, strongly influenced by the presence of a negative charge at P9 unlike clone 72.10 (Figure 3, C and D). TCR 21.30 was approximately 100 times more sensitive to HEL$_{11–27}$ than HEL$_{11–27}$9E. The TCR α and β chains of these clones were isolated by RT-PCR, sequenced, and used to produce recombinant soluble TCR molecules suitable for structural studies.

It was noteworthy that TCR 21.30 had a negatively charged residue (Aspβ109) at position 3 of its CDR3β loop (WDRAGNTL). The exact mode of how TCR 21.30 could be sensitive to position P9 remained unclear until we obtained the crystal structure of TCR 21.30 in complex with I-A^{g7}HEL$_{11–27}$ at a nominal resolution of 3.5 Å (Supplemental Table 8).

Structure of TCR 21.30/I-A^{g7}HEL$_{11–27}$ complex reveals a canonical mode of recognition. TCR 21.30 straddles I-A^{g7}HEL$_{11–27}$ in a central position with its long axis forming a 48° angle with the MHC axis along the binding groove (Figure 4, A and B). This docking mode disproved the hypothesis, at least for this TCR, that the TCR had significantly shifted along the pMHC groove to engage the P9 region in a classic charge-charge interaction. Further, TCR 21.30 did not directly recognize the P9 pocket (Figure 4A and Figure 5A) and only made tangential contact with the backbone of the P9 residue (Figure 5B) via the CDR3β loop residue Trpβ108. The exact role of Aspβ109 in the recognition of the I-A^{g7} P9 pocket is complicated by the fact that its primary contact is to the peptide HEL$_{11–27}$ Arg P8 (Figure 5B). This interaction and, in particular, the salt bridge formed between Aspβ109 and HEL Arg P8 clearly represented a focal point for TCR 21.30 recognition of I-A^{g7}HEL$_{11–27}$. In addition, Aspβ109 is separated from Argα76 (i.e., the P9 pocket) by approximately 12.5 Å and thus does not make direct contact. The sensitivity of TCR 21.30 toward the status of the P9 pocket (i.e., charged or noncharged) can be explained by 2 models. First, a negatively charged P9 residue could modulate TCR 21.30 reactivity via secondary effects on the positively charged peptide Arg P8 residue. In this scenario, favorable electrostatic interactions between Arg P8 and Glu P9 would cause a reduction in the affinity between TCR 21.30 and I-A^{g7}HEL$_{11–27}$9E. It remains unknown, in this situation, whether the side chain of Arg P8 undergoes conformational changes. An alternate model envisages that TCR 21.30 is directly seeing the P9 region of I-A^{g7} (particularly Argα76) via favorable long-range electrostatic interactions. The addition of a negatively charged P9 peptide residue weakens this interaction and hence reduces the affinity of the interaction between TCR and MHC. Although the former model appears most likely, since Arg P8 is clearly a critical residue for TCR 21.30 recognition, it is not possible yet to discriminate between these 2 scenarios.

Another interesting feature of the TCR 21.30 footprint over I-A^{g7}HEL$_{11–27}$ (Figure 4B) was the unusual placement of the CDR3α and CDR3β loops, both of which point outward and away from position P5 of the peptide. The CDR3α loop has a minimal role in peptide recognition (2 contacts with P2 and 7 contacts with P-1), possibly due to the tip of the loop being composed of small residues (GGSG). In contrast, CDR3β appears focused on the C-terminal residues P7, P8, P9, and P11 and to a lesser extent on I-A^{g7} residues (Tyrβ60, Tyrβ66, and Argβ70) located in the β1 α-helix (Supplemental Table 9). This particular docking mode still allowed the P5 side chain to be recognized by Lysα37 (CDR1α) and Argβ110 (CDR3β) (Supplemental Table 9). Even though it resides far from the P9 region (Figure 4A), CDR3β, by pointing outward, contacts not only MHC residues but, more importantly, senses, via Trpβ108 and Aspβ109, the C-terminal P7, P8, P9, and P11 residues of the HEL$_{11–27}$ peptide and the surrounding MHC groove (Supplemental Table 9 and Figure 5B).

Functional studies correlate P9 negative charge with low-affinity TCR 21.30 recognition. We tested the relative importance of the HEL$_{11–27}$ peptide P5, P8, and P9 positions using peptide variants in T cell 21.30 hybridoma stimulation assays (Figure 6). Substituting the P5 Asp residue with an Asn (removal of charge) was tolerated, although the peptide half-maximal effective concentration (EC$_{50}$) was increased approximately 100-fold. However, removing the P5

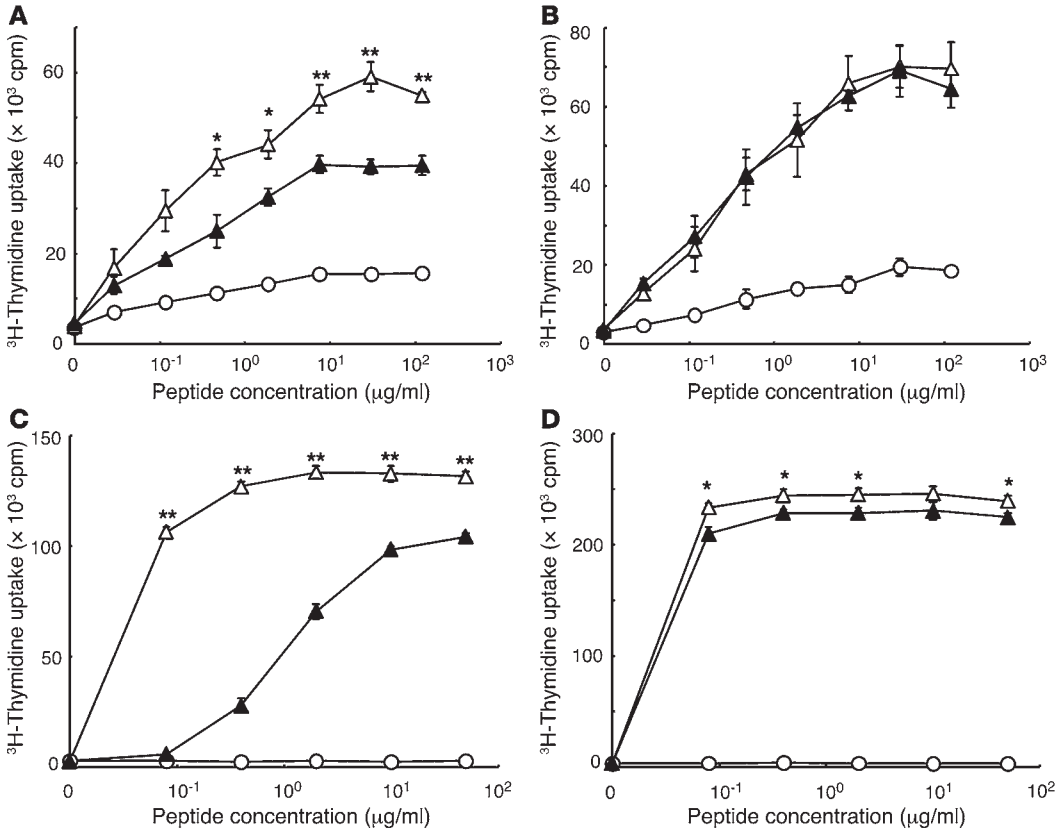

Figure 3

T cell recall response against $HEL_{11–27}$ or $HEL_{11–27}$9E peptides. Polyclonal $CD4^+$ T cell response against $HEL_{11–27}$, $HEL_{11–27}$9E, or control peptide after immunization with (**A**) $HEL_{11–27}$ or (**B**) HEL $HEL_{11–27}$9E. (**C**) T cell hybridoma 21.30 response to $HEL_{11–27}$ or $HEL_{11–27}$9E peptides. (**D**) Response profile of clone 72.10, a T cell that was raised against $HEL_{11–27}$9E. $HEL_{11–27}$, open triangles; $HEL_{11–27}$9E, filled triangles; control peptide, circles. *$P < 0.05$; **$P < 0.01$.

side chain by introducing a glycine abrogated I-$A^{g7}HEL_{11–27}$ recognition by TCR 21.30 and demonstrated that P5 Asp remains a crucial residue for TCR 21.30 binding. The importance of P8 was shown by the fact that the conservative substitution of Lys for Arg caused the EC_{50} to increase approximately 10-fold. Furthermore, truncation of the P8 side chain with a P8 Ala substitution abolished TCR 21.30 recognition. We also demonstrated that position P9 and the last 5 residues of HEL were not needed for TCR 21.30 binding to I-$A^{g7}HEL_{11–27}$. First, a HEL peptide truncated after P8 ($HEL_{11–21}$) still stimulated TCR 21.30 better than a $HEL_{11–27}$9E peptide (Figure 6). Second, a redesigned recombinant pMHC molecule in which segment 23–27 of HEL_{WT} was replaced with a $(GS)_3$ linker sequence stimulated TCR 21.30 as well as I-$A^{g7}HEL_{11–27}$, suggesting that the contacts between CDR3β Trp108 and P11 were not contributing significantly to the binding energy (Figure 7).

The striking dichotomy that TCR 21.30 displays in its response to substitutions at position P9 of the peptide was further documented by using other neutral P9 residues, such as Asn, Gln, and Met (Figures 6 and 7), which all displayed activation profiles similar to that observed for $HEL_{11–27}$. In contrast, negatively charged P9 residues (i.e., Asp or Glu) were recognized with reduced affinity (Figure 7). Interestingly, stimulation of clone 21–30 with I-$A^{g7}HEL_{11–27}$ molecules, where Serβ57 was mutated to an Asp, also resulted in an activation profile similar to that observed for I-$A^{g7}HEL_{11–27}$9E (Figure 8). Together these results suggest that the affinity of TCR/pMHC recognition could be switched from low to high based upon whether Argα76 was paired with a neighboring negatively charged residue.

TCR affinity correlates with peptide charge at P9. The respective roles of ionic strength and conformation on TCR 21.30 affinity were investigated by measuring TCR/pMHC kinetics using surface plasmon resonance (SPR). Substitution of $HEL_{11–27}$ P9 Gly → Glu reduced the TCR/pMHC affinity by approximately 30-fold with a penalty for both the kinetic on and off rates (Figure 9A and Supplemental Table 10) and in essence mirrored the functional data (Figure 6). This difference in affinity approximately corresponds to a –2 kcal/mol difference between the 2 TCR/pMHC complexes in the Gibbs free energy of binding. To put in context, this difference in binding energetics is of the same order of magnitude as the formation of a strong salt bridge (3–6 kcal/mol) (13). A comparable reduction in affinity was also observed for TCR 21.30 binding to I-$A^{g7}HEL_{11–27}$ with a Serβ57Asp (Figure 9B) mutation. Once again, TCR 21.30 recognition of I-A^{g7} is clearly affected by the presence of a negative charge in the P9 pocket. A mutant TCR 21.30 with a CDR3β Asp109Gly mutation also bound I-$A^{g7}HEL_{11–27}$ with reduced affinity (Figure 9A), emphasizing the importance of Aspβ109 for TCR 21.30 binding.

The off rate of the TCR 21.30/I-$A^{g7}HEL_{11–27}$ complex is approximately 6.7 times slower compared with 21.30/I-$A^{g7}HEL_{11–27}$9E (Supplemental Table 10) and directly attributable to the P9

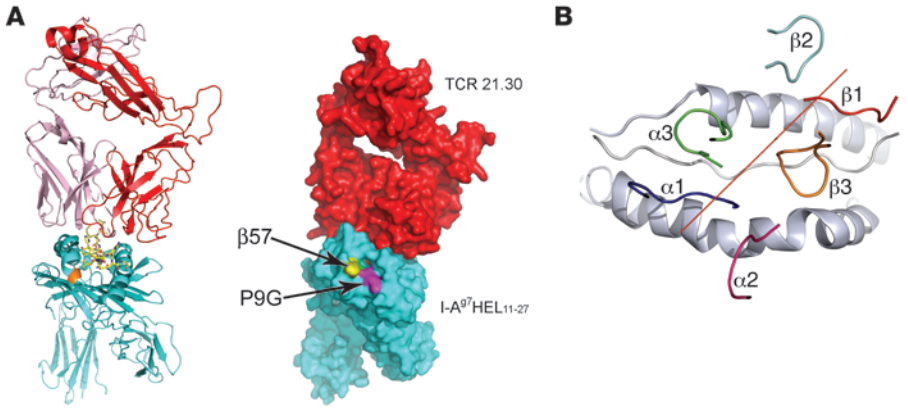

Figure 4
Overview of the TCR 21.30/I-$A^{g7}$$HEL_{11–27}$ complex. (**A**) Ribbon trace of the complex (left). The TCR 21.30 α and β chains are colored pink and red respectively. I-A^{g7} is colored turquoise, except for residue β57 (orange). The HEL peptide is shown as ball-and-stick. Right panels shows the same view, with a space-filling representation showing that both β57 and the P9 pocket lie outside of the TCR footprint. (**B**) Diagonal orientation and footprint of the 6 CDRs of TCR 21.30 on pMHC. The red line denotes the relative diagonal orientation of the TCR to pMHC and is the linear fit to the centers of gravity of the conserved $V_\alpha V_\beta$ sulfurs. The I-A^{g7} α helices, which form the walls of the peptide-binding groove, are drawn as cartoon representations and are colored silver.

Gly → Glu mutation in the peptide. This substitution, therefore, destabilizes the resulting complex, probably due to electrostatic effects. Likewise, the faster on rate of I-$A^{g7}$$HEL_{11–27}$ as compared with I-$A^{g7}$$HEL_{11–27}$9E was suggestive of an increase in favorable Coulombic electrostatic forces (14–16) and directly attributable to the absence of negative charge at P9. The main TCR contributors of this long-range electrostatic interaction appeared to be Aspβ37 and Aspβ109.

The role of electrostatics in recognition was tested directly by measuring TCR/pMHC interaction kinetics in the presence of increasing concentrations of salt. As shown in Figure 9D, increasing concentrations of NaCl lowered the affinity of both I-$A^{g7}$$HEL_{11–27}$ and I-$A^{g7}$$HEL_{11–27}$9E. However, the reduction in affinity for I-$A^{g7}$$HEL_{11–27}$9E was mostly accounted for by a faster off rate, whereas the drop in affinity for I-$A^{g7}$$HEL_{11–27}$ was entirely associated with a slowing of the on rate. As expected, I-$A^{g7}$$HEL_{11–27}$ Aspβ57 behaved comparably to I-$A^{g7}$$HEL_{11–27}$9E (data not shown). These experiments supported the hypothesis that the fast on rate and high affinity of TCR 21.30 for I-$A^{g7}$$HEL_{11–27}$ was driven mainly by electrostatic forces linked to the absence of a negatively charged residue at, or near, P9 and the corresponding presence of negatively charged residues on TCR. Therefore, we have identified in this particular MHC/TCR pair a switch between normal and high affinity that is linked to a non-TCR contact residue on the peptide and a CDR3β negatively charged amino acid. The presence of the same feature in polyclonal populations specific for antigens bearing no charge at P9, as suggested by our functional data, argues strongly against an alternate explanation involving conformational changes of the TCR.

Discussion

A single residue polymorphism of MHC class II gene products dominates the genetic makeup of T1D and other autoimmune conditions such as celiac disease (17). A correlation between the absence of an aspartate residue at position 57 of the MHC β chain and susceptibility to T1D was first noted over twenty years ago (3). Biophysical and structural studies have since ruled out the possibility that the loss of the salt bridge between Argα76 and β57 was detrimental to either the integrity of I-A^{g7} or its capacity to bind peptide (4–6). It remains clear, however, that the absence of a negative charge in this region of the I-A^{g7} leads to the preferential binding of peptides carrying an Asp or Glu at position P9 of the peptide groove (4, 5, 18). Nevertheless, the I-A^{g7} binding motif is sufficiently promiscuous to allow binding of peptides containing a neutral residue at P9 (4, 5). Upon binding, these neutral peptides cause the P9 region of the I-A^{g7} binding groove to be more positively charged due to the presence of the unpaired Argα76. We have now examined the consequences of this unique feature on the selection of TCR repertoire against I-A^{g7} neutral P9 peptides.

Our results, obtained from 3 distinct antigenic systems, convincingly demonstrate that in the absence of Asp/Glu P9 residues, selected TCRs have a strong tendency to have Asp/Glu residues in CDR3β. A remarkably similar observation was also reported in 2 earlier studies that examined the T cell repertoire of $CD4^+$ T cells infiltrating the pancreas of young NOD mice. Here, in both cases, a similar signature was detected whereby the number of TCRs with Asp and Glu residues in the N-terminal region of their CDR3β was increased (19, 20). We have also recently reported the same feature for the recognition of HLA-DQ8 native gliadin peptide complexes in which the P9 residue is Gln (10).

Mechanistically, the structure of TCR 21.30/I-$A^{g7}$$HEL_{11–27}$ disproved our initial idea that the TCR had to shift toward the P9 pocket in order to recognize I-A^{g7} with an uncharged P9 residue and also showed that a noncontact residue could heavily influence TCR recognition. This mode of recognition for TCR 21.30 does not rule out the possibility that direct recognition of the P9 patch could be accomplished directly by other TCRs (in an analogous manner to that observed for the I-$A^{g7}$$GAD_{221–235}$ dimer). However, we believe that our proposed switch would be unlikely to function in this scenario since the P9 position would be expected to function as a surrogate P5 residue, i.e., any significant substitutions at P9 (e.g., Gly Glu) would now be expected to result in loss of TCR recognition. Biophysical and functional activation studies of TCR 21.30 binding revealed that the absence of negatively charged P9 peptide residue resulted in a 30-fold increase in affinity due to increased favorable electrostatic interactions. More importantly, our study of both the HEL and 2.5mi antigenic systems showed that the potential gain in TRC/pMHC affinity provided by the lack of charge at P9 and negative charge on CDR3β translated into higher proliferation and increased expansion in vivo (Figure 10).

In I-A^{g7}, the presence of a neutral Ser residue at position β57 creates a switch with the potential to modulate TCR affinity. At least 2 models can be proposed by which this switch may function. First, a

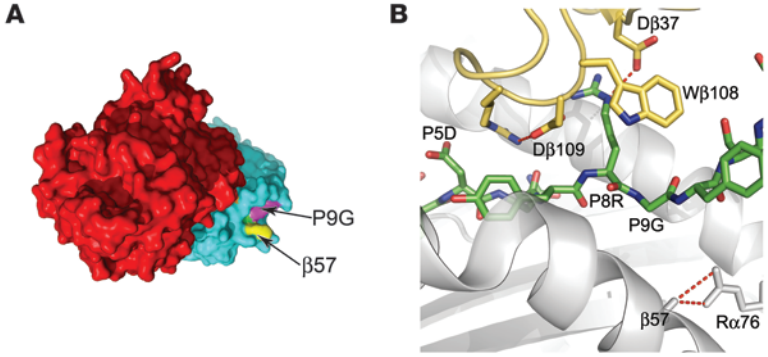

Figure 5
TCR 21.30/I-A^{g7}HEL$_{11–27}$ structure. (**A**) Space-filling view of the complex, looking from behind the TCR and down toward the MHC, highlights how far β57 and P9 are from the TCR-binding interface. (**B**) The CDR3β loop points outward toward the P9 pocket and C terminus of the peptide. However, the main focus of CDR3β remains peptide residue Arg P8.

"direct model" envisages that TCR and in particular CDR3β see the P9 region directly via favorable long-range electrostatic interactions, although the possibility exists that longer CDR3β loops may still make direct contact with the P9 pocket. Replacement of the peptide P9 residue with a negatively charged residue breaks or weakens the aforementioned TCR-pMHC electrostatic interaction and hence causes a reduction in the resulting affinity. Our data suggest that the GAD$_{221–235}$ and 2.5mi antigenic systems would be good examples of this "direct model." A second "indirect model" envisages that TCR recognition is heavily influenced by a positively charged peptide residue at P8 (e.g., Arg/Lys) via favorable electrostatic interactions and that the neighboring P9 residue dictates the strength of the electrostatic interaction between P8 and TCR CDR3β by having no impact (neutral residues) or a competing deleterious effect (Asp/Glu).

It is important to emphasize that both models establish the notion of an I-A^{g7} switch located at residue β57. Further, these models demonstrate the uniqueness of β57 by highlighting its dual role in defining peptide specificity and modulating TCR affinity.

Is this switch model or models applicable to the human homolog of I-A^{g7}, namely HLA-DQ8? We have recently shown for celiac disease (10) that TCRs raised against HLA-DQ8 and native gluten peptide (with a neutral Gln P9 residue) do indeed have a preponderance of

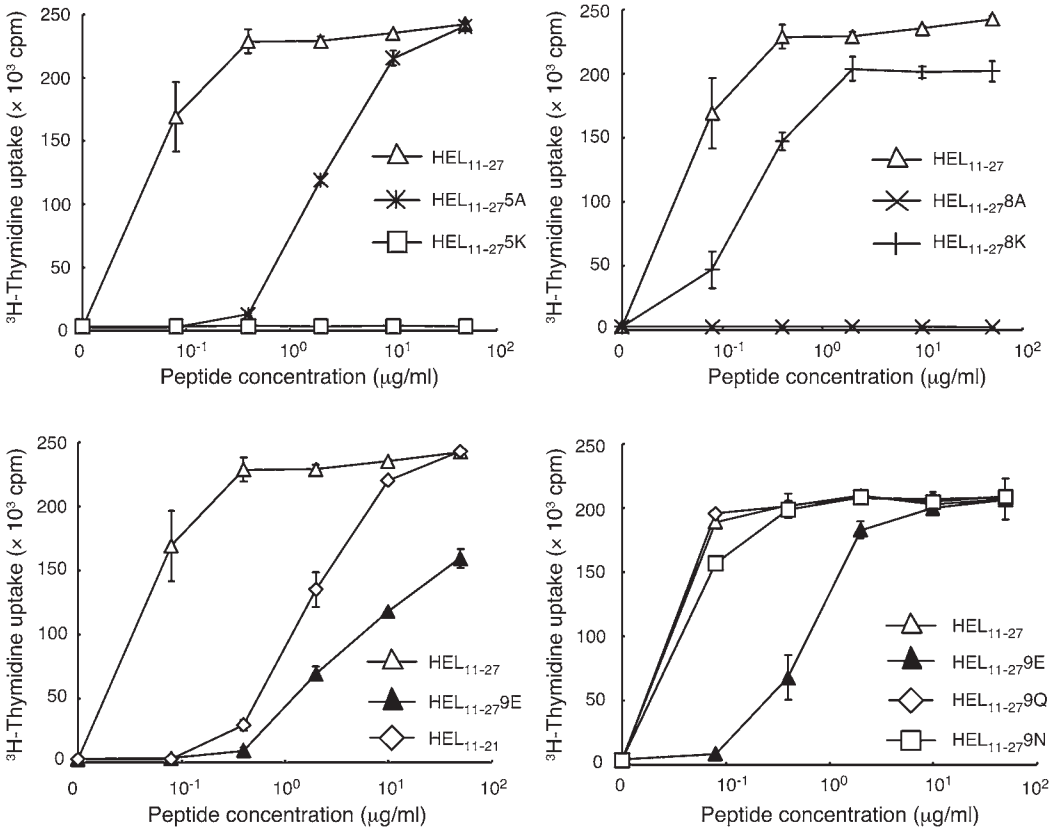

Figure 6
Reactivity of clone 21.30 to stimulation by mutant HEL peptides. HEL$_{11–27}$ mutations at positions P5, P8, and P9 as well as a truncated HEL peptide (HEL$_{11–21}$) were tested at various concentrations in a classic T cell presentation assay using irradiated splenocytes as APCs and clone 21.30 as responder cells. IL-2 release was measured using an IL-2 reporter cell line. Each assay was repeated at least twice. A representative experiment is shown. Values are mean of triplicates ± SD.

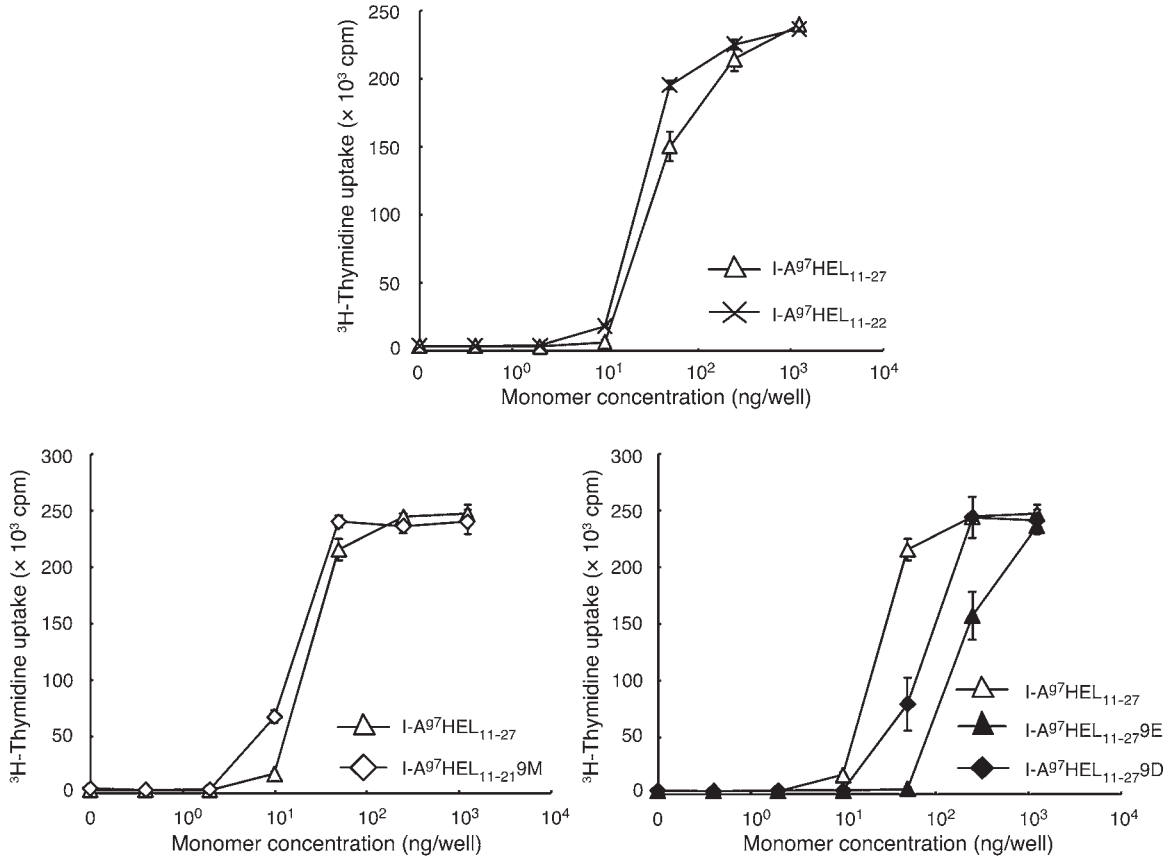

Figure 7
Stimulation of clone 21.30 with I-$A^{g7}$$HEL_{11–27}$ or I-$A^{g7}$$HEL_{11–27}$ P9 mutants or truncated I-$A^{g7}$$HEL_{11–22}$. MHC peptide complexes were coated in 96-well plates at increasing concentrations and used to stimulate clone 21.30 overnight. IL-2 production was measured using an IL-2–dependent reporter line. Values are the mean of triplicates ± SD.

Asp/Glu residues in CDR3β when compared with TCRs raised against deamidated gluten peptide (Glu at P9). This observation strongly suggests that a similar mechanism may be functioning for HLA-DQ8.

An important unanswered question is why would the switch act differently in the thymus and in the periphery? The answer is that it probably does not. However, in the thymus, T cells endowed with a potential switch will be deleted when selected on peptides with neutral P9 residues (negative selection). On the other hand, a number of thymic emigrant T cells with potential switches (e.g., most Vβ8-bearing cells) will be selected on peptides with an Asp/Glu P9 residue and access the periphery where an encounter with a peptide having a neutral P9 residue will make them potentially dangerous by increasing their affinity and lessening their MHC and coreceptor threshold. The thymic selection of BDC 2.5 T cells on mutant I-A^{g7} PD MHC (in which positions β56 and β57 are Pro and Asp, respectively) paired with the failure of I-A^{g7} PD to present pancreatic antigens to BDC 2.5 T cells (21) argues strongly in favor of this hypothesis by demonstrating that the β57 mutation is required only for T cell activation in the periphery and not the thymus. An alternative nonexclusive explanation is that very small "switch populations" arise and expand over time in the periphery through antigen-driven affinity maturation (22); the results in the BDC 2.5 system that showed the predominance of junctional editing in the coding of CDR3β Asp/Glu residues support such a scenario.

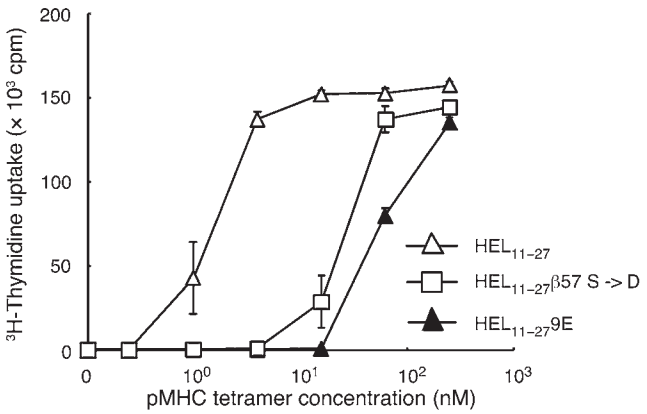

Figure 8
Reactivity of clone 21.30 to I-A^{g7} with a β57 S → D mutation. A negatively charged residue introduced into either the peptide and/or the MHC has similar consequences for the activation and affinity of T cell clone 21.30. Stimulation of clone 21.30 with pMHC molecules bound to the surface of culture plates. Tetramized molecules of $HEL_{11–27}$ peptide or its 9E mutant in the context of I-A^{g7} or the I-A^{g7} β57 S → D mutant were used to stimulate clone 21.30 overnight. IL-2 production was measured using an IL-2–dependent reporter cell line. Values are the mean of triplicates ± SD.

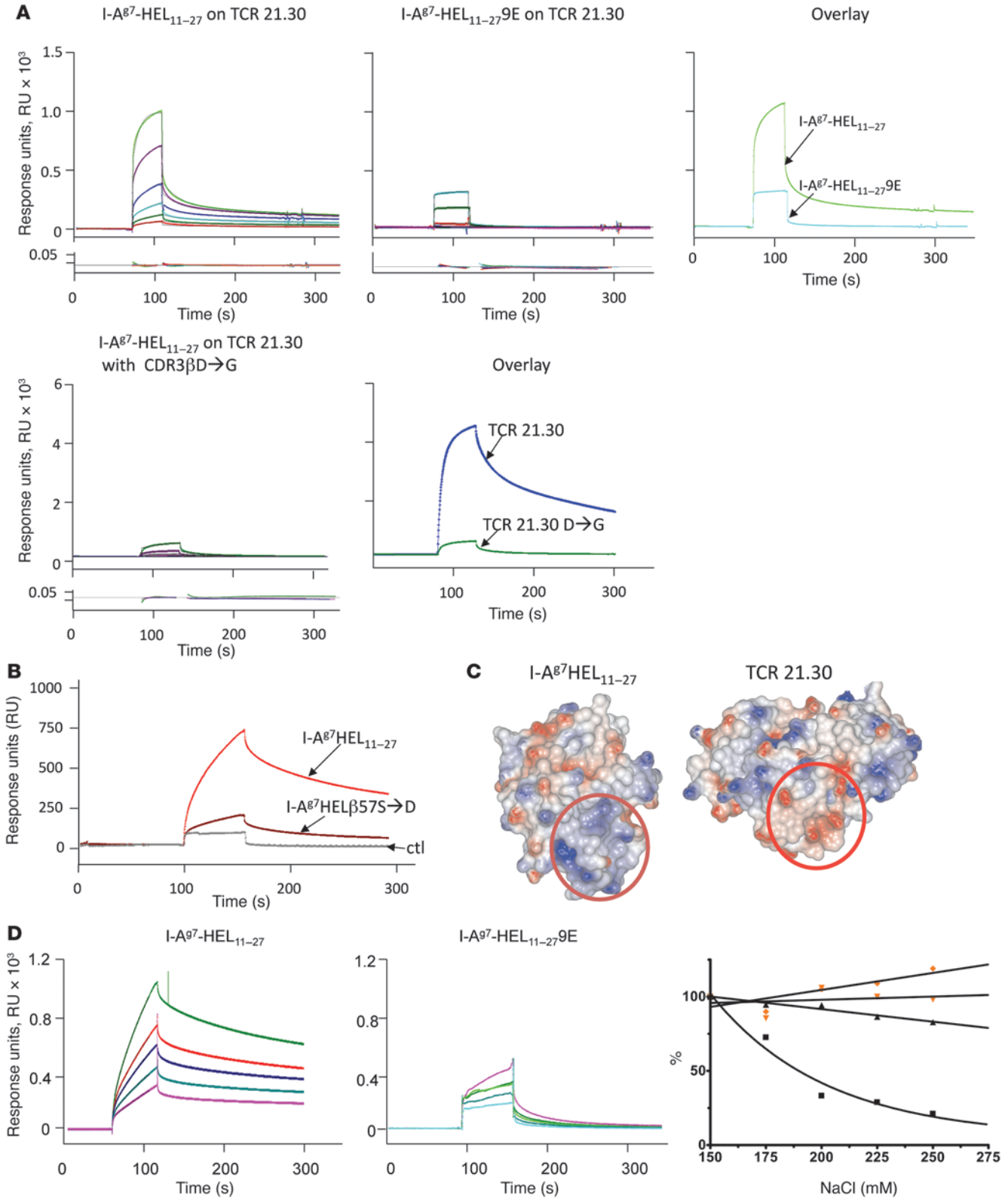
A
I-Ag7-HEL11–27 on TCR 21.30
I-Ag7-HEL11–27 9E on TCR 21.30
Overlay
Response units, RU × 10³
Time (s)
I-Ag7-HEL11–27
I-Ag7-HEL11–27 9E
I-Ag7-HEL11–27 on TCR 21.30 with CDR3βD→G
Overlay
TCR 21.30
TCR 21.30 D→G
B
Response units (RU)
I-Ag7HEL11–27
I-Ag7HELβ57S→D
ctl
C
I-Ag7HEL11–27
TCR 21.30
D
I-Ag7-HEL11–27
I-Ag7-HEL11–27 9E
%
NaCl (mM)

Figure 9
SPR affinity measurements between TCR/pMHC. (**A**) Affinity measurements of TCR 21.30 for I-A^{g7}HEL$_{11–27}$ and I-A^{g7}HEL$_{11–27}$9E (top) and TCR 21.30 CDR3β 109 D → G and I-A^{g7}HEL$_{11–27}$ (bottom) (pMHC molecules were injected at 5, 2.5, 1.25, 0.625, 0.312, and 0.187 μM over immobilized TCR). Sensorgrams represent specific binding after subtraction of control (I-A^{g7} 2.5mi) and were fitted using global analysis with the BIAcore software using a 1:1 Langmuir model (residuals are shown below the sensorgrams). Overlays are at 5 μM. (**B**) SPR measurement of the affinity of recombinant TCR 21.30 for I-A^{g7}HEL$_{11–27}$ and I-A^{g7} β57 S → D HEL$_{11–27}$. TCR was immobilized on a CM5 chip (1200 RUs), and pMHC molecules were injected at 2 μM concentration. Sensorgrams presented in the figure are the subtraction of the experimental trace minus the negative control (I-A^{g7} 2.5mi). (**C**) Electrostatic surfaces of I-A^{g7}HEL$_{11–27}$ (left) and TCR 21.30 (right) showing charge complementarity between the 2 surfaces. TCR has been "peeled off" the MHC (180° rotation) to reveal the interacting surfaces. The corresponding positive (pMHC, blue) and negative (TCR, red) surfaces are circled. Positive charge is contoured blue, while negative charge is red (–5 to +5 kT/e). (**D**) Effect of increasing salt concentrations on the binding of I-A^{g7}HEL$_{11–27}$ (black) and I-A^{g7}HEL$_{11–27}$9E (red) to TCR 21.30. I-A^{g7}HEL$_{11–27}$ was injected at 2 μM and I-A^{g7}HEL$_{11–27}$9E at 8 μM with increasing NaCl concentrations (150, 175, 200, 225, and 250 mM NaCl). Sensorgrams are double subtractions (control pMHC and buffer). Kinetic on (squares or upside-down trangles) and off rates (triangles or diamonds) are plotted relative to physiological ionic conditions (150 mM). Representative experiments are presented (n = 5).

The MHC class II region dominates the genetic landscape of T1D (17). This strong association has, for many years, suggested that T1D-associated MHC class II molecules have a direct role in the disease pathogenesis. The prevention of diabetes onset by the introduction of an I-A^{g7} β57 S→D mutant in transgenic NOD mice (23) supports this idea. Here, for what we believe is the first time, we have shown that the diabetogenic MHC I-A^{g7} has a unique molecular signature that is directly linked to the polymorphic residue β57. The critical issue of testing the relationship of our switch model to autoimmunity now needs to be addressed.

Methods

Immunization. NOD/LtJ mice were purchased from Jackson Laboratories and housed in pathogen-free conditions. For in vivo T cell response studies, mice were immunized in the base of the tail and the foot paw with 5 μg of peptide reconstituted in PBS and emulsified in complete Freund's adjuvant (Sigma-Aldrich). Animals were sacrificed between 3 and 12 days following immunization. All experimental procedures involving animals were performed according to institutional guidelines of The Scripps Research Institute and were approved by the Institutional Animal Care and Use Committee of The Scrips Research Institute.

Cells. BW5147 (TCR$^{α–β–}$) cells and T cell hybridomas were maintained in DMEM/10% FCS medium.

Peptides. Synthetic peptides, 2.5mi 9D (AHHPIWARMDA), 2.5mi 9Q (AHHPIWARMQA), 2.5mi 5G 9D (AHHPIGARMDA), 2.5mi 5G 9Q (AHHPIGARMQA), GAD$_{221–235}$ (LKKMREIIGWPGGSG), GAD$_{221–235}$9E (LKKMREIIGWPEGSG), HEL$_{11–27}$ (AMKRHGLDNYRGYSLGN), HEL$_{11–27}$9E (AMKRHGLDNYREYSLGN), HEL$_{11–27}$5G (AMKRHGLGNYREYSLGN), HEL$_{11–27}$5N (AMKRHGLNNYRGYSLGN), HEL$_{11–27}$8A (AMKRHGLDNYAGYSLGN), HEL$_{11–27}$8K (AMKRHGLDNYKGYSLGN), and HEL$_{11–21}$ (AMKRHGLDNYR) were greater than or equal to 95% pure and synthesized by AnaSpec Inc.

Establishment of T cell hybridomas. Lymphocytes from peptide-immunized mice were stimulated in vitro with peptide for 4 days and then stimulated with concanavalin A (2 μg/ml) for a further 3 days. After washing, cells were mixed with BW5147 in 50% w/v polyethylene glycol (PEG) solution (Hybrimax; Sigma-Aldrich). After culturing with hypoxanthine/aminopterin/thymidine media, T cell hybridomas were tested for reactivity to peptide with γ-ray–irradiated NOD splenocytes (antigen-presenting cells) by measuring the amount of IL-2 released for 24 hours. IL-2 production was determined using the IL-2–dependent cell line NK. The hybridomas from positive wells were expanded and cloned at 0.3 cells per well.

To test the response of T cell hybridomas against I-A^{g7} peptide complexes, 96-well flat-bottom plates (Corning Inc.) were coated with serially diluted MHC/peptide complexes in PBS overnight at 4°C and washed 3 times with PBS. T cell hybridomas were washed twice in PBS, resuspended in complete DMEM, and added at 5 × 10^4 cells per well in 200 μl for 24 hours at 37°C. To test the response of T cell hybridomas against tetramer of I-A^{g7} peptide, T cell hybridomas were cultured with the tetramers for 24 hours at 37°C. Supernatants were harvested and IL-2 production determined using the NK cell line. ^{3}H-thymidine uptake was determined by liquid scintillation analysis and expressed as cpm.

RNA extraction and RT-PCR. Total RNA from T cell hybridomas was isolated with TRIzol (Invitrogen), and Moloney murine leukemia virus (MMLV) (Invitrogen) was used for reverse transcription according to the manufacturer's instruction.

Construction, expression, and purification of recombinant TCR, and I-A^{g7}/peptide molecules; generation of tetrameric MHC molecules. TCR cDNA for the α and β chains of the HEL$_{11–27}$–reactive T cell hybridoma (clone 21-30-7) were obtained by RT-PCR. Oligo dT primers (GE Healthcare) as well as sequence-specific primers (Vα11-5, 5′-AAAAAGAATTCGAAATGSAGAGGAACCTGGKWGCTG-3′; Vβ8.1-5, 5′-AAAAAGAATTCGAAATGGGCTCCAGACTCTTCTTTG-3′; Cα-3, 5′-CTTTGAAGATATCTTGGCAGG-3′; Cβ-3, 5′-CCCATGGAACTGCACTTGGCAG-3′) were used for cDNA synthesis and PCR amplification, respectively. PCR products were subcloned into the fly expression vector pRMHa3 or pMT/Bip/V5-His (Invitrogen) and sequenced. The final constructs coded for the $\alpha_1\alpha_2$ and the $\beta_1\beta_2$ domains, respectively, followed by a linker sequence (SSADL), a thrombin site (LVPRGS), a leucine zipper (acidic for the α chain, basic for the β chain), and a hexahistidine tag. A variant of this TCR bearing an additional disulfide bridge between the Cα-Cβ domains was also produced for crystallization studies (24). Vectors were cotransfected into SC2 cells along with a vector encoding a puromycin-resistance gene, and stable cell lines were established. Soluble TCRs were purified from culture supernatants, as previously described (25).

The generation of I-A^{g7}/peptide complexes has been reported in detail (5). The peptide sequences of I-A^{g7}/2.5mi 9D, I-A^{g7}/2.5mi 9G, I-A^{g7}/2.5mi 9Q, I-A^{g7}GPI$_{282–292}$, I-A^{g7}HEL$_{11–27}$, I-A^{g7}HEL$_{11–27}$9E, I-A^{g7}HEL$_{11–27}$9D, I-A^{g7}HEL$_{11–27}$9M, I-A^{g7}HEL HEL$_{11–22}$, and I-A^{g7}HEL$_{11–22}$9E molecules are AHHPIWARMDA, AHHPIWARMGA, AHHPIWARMQA, LSIALHVGFDH, AMKRHGLDNYRGYSLGN, AMKRHGLDNYREYSLGN, AMKRHGLDNYRDYSLGN, AMKRHGLDNYRMYSLGN, AMKRHGLDNYRG, and AMKRHGLDNYRE. respectively. The biotinylation sequence no. 85 from Schatz (26) follows the acidic zipper on the α chain. Biotinylation of purified I-A^{g7} molecules was performed according to the manufacturer's instructions. Biotinylated molecules were tetramerized at 4°C overnight using PE-labeled (BioSource International) or PE–cyanine 7–labeled streptavidin (eBioscience) using a 5:1 molar ratio of biotinylated molecules to labeled streptavidin.

Site-directed mutagenesis. PCR site-directed mutagenesis was carried out using PfuUltra High-Fidelity DNA Polymerase (Stratagene).

Cell preparation, cell staining, and flow cytometry analysis. Single-cell suspensions were prepared by mechanical disruption of the corresponding organs in HBSS buffer, and erythrocytes were removed by lysis. Cells were

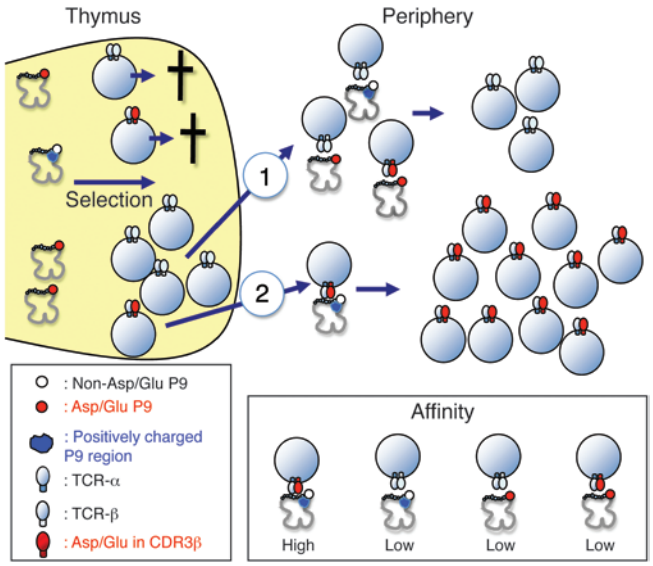

Figure 10
Potential consequences of I-A^{g7} being endowed with a switch that modulates TCR affinity. TCRs are selected normally in the thymus against I-A^{g7} peptide complexes and the encounter of TCR with an Asp/Glu-containing CDR3β region with a neutral P9 peptide leads to negative selection. However, a small fraction of those same TCRs will be positively selected against pMHC with an Asp/Glu P9 peptide and migrate out of the thymus. In the periphery, normal recognition will occur in a majority of cases, followed by a normal burst of proliferation after recognition of pMHC (scenario no. 1). The exception (scenario no. 2) will happen when a TCR with an Asp/Glu-containing CDR3β detects a pMHC complex displaying a neutral P9 residue; in that instance, increased affinity will lessen pMHC and coreceptor threshold for activation and lead to increased expansion and potentially increased cytokine secretion.

washed with FACS buffer (PBS containing 3% FCS and 0.05% NaN_3) and incubated with 0.5 mg/ml of avidin (Sigma-Aldrich) and Fc block (BD Biosciences) in FACS buffer for 1 hour at room temperature (RT). Cells were then washed once and stained with PE-labeled or PE–cyanine 7–labeled MHC/peptide tetramers at a final concentration of 10 μg/ml in FACS buffer for 1 hour at RT. For costaining of surface markers, FITC–anti-CD4 (clone RM4-4; BD Biosciences), allophycocyanin–anti-B220 (clone RA3-6B2; eBioscience), and allophycocyanin–anti-CD8 (clone 53-6.7; eBioscience) were used. For TCR Vβ analysis, mouse Vβ TCR screening panel (BD Biosciences) was used. Exclusion of dead cells was done by propidium iodide (Invitrogen). Flow cytometry was performed using a FACS LSR-II instrument or FACSCalibur (BD) and the data analyzed using FlowJo software (TreeStar Inc). Staining of T cell hybridomas with MHC tetramers was carried out in the same way.

CD4$^+$ T cell response. For purification of CD4$^+$ T cells, lymph node or spleen cells from immunized mice were incubated with Fc block for 1 hour at 4°C. Cells were then incubated with biotinylated anti-CD8a (clone 53-6.7), biotinylated anti-CD11b (clone M1/70), biotinylated anti-CD45R (B220; clone RA3-6B2), biotinylated anti-CD49b (clone; HMa2), biotinylated anti-TER119 (clone TER-119; eBioscience), and biotinylated anti-major histocompatibility complex class II (clone AMS-32.1; BD Biosciences). After washing, cells were incubated with Streptavidin Particles Plus-DM (BD Biosciences) and CD4$^+$ T cells were enriched by negative selection with BD IMag Cell Separation System (BD Biosciences). The percentage of CD4$^+$ T cells after purification was confirmed by flow cytometric analysis. CD4$^+$ T cells (4×10^5) were cultured with peptide and 2×10^5 cells of γ-ray irradiated splenocytes derived from NOD for 72 hours. ^{3}H-Thymidine was added during the last 16-18 hours of culture. For measurement of IFN-γ, the cell culture supernatants were collected after 48 hours incubation. The amount of IFN-γ was determined by ELISA (Opti EIA; BD Biosciences) following the manufacturer's protocol.

Single-cell PCR and CDR3β sequencing. Single-cell suspensions from immunized or naive NOD mice were prepared by mechanical disruption in the same way as the cell staining. Cells were washed with sorting buffer (PBS containing 1% FCS, 1 mM EDTA, and 25 mM HEPES) and incubated with avidin and Fc block. After washing, the cells were stained with PE-labeled or PE–cyanine 7–labeled MHC/peptide tetramers. Cells were then stained with FITC–anti-CD4, allophycocyanin–anti-B220, and allophycocyanin–anti-CD8. Enriched CD4$^+$ T cells, which were prepared in the same way as in the experiments for CD4$^+$ T cell responses, were also used for tetramer and antibody staining. The single tetramer-positive CD4$^+$ T cell was directly sorted into cDNA reaction mixture of 96-well PCR tubes by FACSVantage DiVa. This reaction mixture contains 3 U/μl MLV-RT (Invitrogen) with × 1 buffer, 0.5 nM spermidine, 0.1 mg/ml BSA, 10 μg/ml oligo d(T), 400 μM each dNTP (Invitrogen), 10 mM dithiothreitol, 800 U/ml ribonuclease inhibitor (recombinant RNasin), 100 μg/ml *Escherichia coli* transfer RNA, and 1% Triton X-100. cDNA was synthesized at 37°C for 75 minutes and 42°C for 30 minutes, then stored at –80°C until use.

PCR amplifications of TCR β chain from cDNA of single tetramer-positive CD4$^+$ T cell was performed by 2 rounds of PCR. After a first round PCR with external mixture coupled with a constant region external primer (Supplemental Table 11 and ref. 19), 2 μl of the first reaction was used for a second round PCR with each internal primer coupled with a constant region internal primer (Supplemental Table 11 and ref. 19). PCR products were checked for size on a 1.5% agarose gel stained with ethidium bromide, purified (QIAquick PCR Purification Kit; QIAGEN), and used for direct sequencing with a constant region internal primer. To examine the accuracy of cell sorting, cDNA was analyzed for PCR with β-actin primers.

CDR3β sequencing by TA cloning. CD4$^+$ T cells from naive NOD mice were prepared in the same way. Total RNA from CD4$^+$ T cells was isolated with TRIzol and cDNA was synthesized using MMLV. PCR amplifications of TCR β chain from cDNA of CD4$^+$ T cells were performed with internal mixture primers coupled with a constant region internal primer. PCR products running between 200 and 500 bp were cut out and gel purified (Gene Clean Kit III; MP Biomedicals LLC). These PCR products were directly ligated into pCR2.1 vector (Invitrogen) and sequencing with M13 reverse primer.

SPR. A BIACORE 2000 instrument was used to determine interactions between purified MHC/peptide complexes and TCR molecules. TCR or pMHC was immobilized by amine coupling chemistry on CM5 sensor chips. Injections of analyte at the appropriate concentrations were performed in filtered and degassed PBS at a flow rate of 20–30 μl/min. In all experiments, I-A^{g7}/GPI$_{282-292}$ was used as a negative control. K_D values as well as on and off rates were obtained by nonlinear curve fitting of subtracted curves using the 1:1 Langmuir binding model using the BIAevaluation program (version 3.0.2).

Statistics. Fisher's exact test and Student's *t* test (2-tailed) were used for statistical analyses. $P < 0.05$ was considered significant.

Crystallization. I-A^{g7}GAD$_{221-235}$ was crystallized after first removing the acidic and basic leucine zippers by thrombin digestion. Residual COOH-terminal spacer sequences were digested with carboxypeptidase B, and

I-A^{g7}GAD$_{221–235}$ was then concentrated to 10 mg/ml in 20 mM HEPES and 25 mM NaCl (pH 7.5) and screened for crystallization. Crystals were grown in 28% PEG 8000, 0.1 M HEPES, pH 7.5, and 2% Jeffamine 900 and flash-cooled to 96 K with glycerol as a cryoprotectant (through a sequential soak in 1%, 5%, 10%, and 15% glycerol).

TCR 21.30/I-A^{g7}HEL$_{11–27}$ was crystallized after first removing the acidic and basic leucine zippers from both constructs by thrombin digestion. TCR and MHC were mixed at a final concentration of 100 μM in 20 mM HEPES, pH 7.5, 100 mM NaCl, and crystallized in 20% PEG4000, 0.2 M K formate, 0.1 M Na cacodylate, pH 6.5. Data were collected on a single crystal cryogenically protected in mother liquor supplemented with 25% glycerol.

Structure determination. A single MHC crystal was used for data collection at beamline 9-2 of Stanford Synchrotron Radiation Lightsource (SSRL). Data were integrated in space group $P4_32_12$ (a = b = 55.83 Å, c = 338.83 Å) with DENZO (version 1.9.1) and reduced with SCALEPACK (version 1.9.0). Crystal mosaicity was refined to 1.2°. A single I-A^{g7} was assumed to be present in the asymmetric unit based on the calculated Matthews' coefficient (V_m ~2.9 Å^3/Dalton, ~58.0% solvent). Molecular replacement was carried out with CCP4's version of *Molrep* (27) and the MHC class II search model I-A^{g7}GAD$_{207–220}$ (Protein Data Bank [PDB] code 1es0), with the waters omitted. A clear rotation (correct solution was found 8.8σ above the next highest peak, resolution 39.2 to 3.1 Å) as well as a translation solution (correct solution was 11.9σ above the next highest peak) was found for I-A^{g7}. Rigid body fitting (6.0 to 3.2 Å) was carried out using the program *CNS* (28) using 3 domains α_1/β_1 plus peptide, α_2, and β_2 to give an R_{cryst} of 37.9%. Model building was carried out using the graphics program *COOT* (29), and iterative refinement cycles were carried out with *Phenix* (30). *CNS* simulated-annealed omit maps and the structure validation programs *Procheck* (31) and *WHATIF* (32) were used to monitor the progress of the refinement (Supplemental Table 7). The final structure contained 2,924 protein atoms, 1 sugar, and 1 HEPES molecule. The following residues were built for I-A^{g7}GAD$_{221–235}$: Ileα1A–Trpα178, Serα179–Alaα181, Gluβ4–Serβ104, Thrβ114–Pheβ132, Gluβ138–Leuβ161, Tyrβ171 to Trpβ188, Lysβ222P–Glyβ235P and Glyβ236P. Density for the first residue of GAD$_{221–235}$ and the loops Argβ105–Asnβ113, Argβ133–Gluβ137, and Gluβ162–Valβ170 were absent and were therefore not modeled. β222P–β235P is the tethered GAD peptide, whereas α179–α181, and β236P are linker residues. The coordinates and structure factors have been deposited in the PDB (code 3CUP).

TCR/MHC complex. Data were collected at the Argonne Advanced Photon Source (APS) beamline 23-ID-B on a MARMOSAIC 300-mm CCD and processed with HKL2000 and XPREP (version 2005/3) with partial data to 2.88 Å resolution in the space-group $P2_12_12_1$ (a = 67.47 Å, b = 99.39 Å, c = 404.68 Å; Supplemental Table 8). The data were highly anisotropic and had a nominal resolution of 3.5 Å. Molecular replacement was carried out using *Phaser* (version 1.3.1) (33). The solvent content was estimated at 60%, suggesting 2 TCR-pMHC complexes per asymmetric unit. Coordinates for I-A^{g7}GPI$_{282–292}$ (A.L. Corper and I.A. Wilson, unpublished observations) were used as a search model for I-A^{g7}HEL$_{11–27}$. A clear solution for the first I-A^{g7}HEL$_{11–27}$ molecule was found (translation Z-score = 17.6, with no other solutions using default selection criteria). The coordinates for 2C TCR (PDB code 1MWA) were used to search for TCR 21.30 (while fixing the solution for I-A^{g7}HEL$_{11–27}$), and a clear solution was obtained (translation Z-score = 15.9; next highest peak = 6.8). A second I-A^{g7}HEL$_{11–27}$ molecule could also be clearly located (translation Z-score = 23.8, with next highest peak = 18.9 with no packing solution). However, the second TCR 21.30 could not be located independently using either *Phaser* or *Molrep* (n.b. *Molrep* was able to locate the 2 I-A^{g7}HEL$_{11–27}$ molecules). The second TCR 21.30 was, therefore, assumed to have the same orientation with respect to its I-A^{g7}HEL$_{11–27}$ binding partner as that observed for the first TCR 21.30. A rotation/translation search using 1 complete TCR-pMHC complex was then used to position the second TCR 21.30. Rigid-body refinement was carried out in *Phenix* (with the HEL peptide residues truncated back to either alanine or glycine as appropriate and the CDRs omitted from the model). The 2C Vα domain was then substituted with the corresponding domain for Vα85.33 (PDB code 1H5B; 75% identity with TCR21.30 over 106 residues). Likewise, the 2C β chain was substituted with the corresponding chain from TCR AHIII 12.2 (PDB code 1LP9; 94% identity with TCR21.30 over 239 residues). Model building was carried out using the graphics program *COOT* (29), and iterative refinement cycles (individual atomic coordinates, restrained NCS, TLS, and grouped B-factor refinement) were carried out with *Phenix* (version 1.5.2) (30). The final few rounds of refinement were carried out using anisotropy-corrected data provided by the diffraction anisotropy server (http:/www.doe-mbi.ucla.edu/~sawaya/anisoscale/). Structure validation programs *Procheck* (31) and *WHATIF* (32) were used to monitor the progress of the refinement (Supplemental Table 8). The coordinates and structure factors have been deposited in the PDB (code 3MBE).

Modeling of I-A^{g7}GAD$_{221–235}$9E. I-A^{g7}GAD$_{221–235}$9E was modeled from I-A^{g7}GAD$_{221–235}$ by mutating the P9 peptide residue from Gly Glu. The Glu side chain was positioned into the P9 pocket of I-A^{g7} using the crystal structure of I-A^{g7}GAD$_{207–220}$ as a guide, since GAD$_{207–220}$ has a Glu at position P9 of the peptide. Restrained energy minimization was then carried out on I-A^{g7}GAD$_{221–235}$9E using the Discover module within Insight II (http://www.accelrys.com/).

Structure analysis. Superimposition of the TCR-pMHC complexes with ProFit (A.C.R. Martin; http://www.bioinf.org.uk/software/profit/) was done using residues in the conserved β-sheet floor of the MHC peptide-binding groove. C_α atoms were used for the superimposition, and the specific residues were α18 to α26, α29 to α34, β24 to β32, and β37 to β42 (Kabat numbering). Molecular surfaces were calculated with a probe radius of 1.4 Å. Electrostatics were calculated with the Delphi module within Insight II. Formal charges were assigned to the protein coordinates. Electrostatic surfaces are contoured from –5 to +5 kT/e; red (negative) to blue (positive), respectively.

TCR and MHC nomenclature. TCR 21.30 V domains were numbered according to the IMGT (http://www.imgt.org) unique numbering for V-REGIONs. KABAT numbering was used for I-A^{g7}.

Acknowledgments

We thank A. Schiefner and R. Stanfield for crystallographic assistance; V. Mallet-Désigné, T. Stratmann, N. Schrantz, S. Freigang, E. Landais, P. Verdino, and M. Hong for advice and discussion; R. Stefanko, C. Puckett, and J. Sim for technical assistance; the Scripps Flow Cytometry Core Facility for cell sorting; and the staff at SSRL beamlines 9-2 and 11-1 for data collection time and assistance. This work was supported by NIH grants CA58896 (to I.A. Wilson) and DK55037 (to L. Teyton).

Received for publication October 20, 2009, and accepted in revised form February 3, 2010.

Address correspondence to: Luc Teyton, Department of Immunology and Microbial Science, or Ian A. Wilson, Department of Molecular Biology and Skaggs Institute for Chemical Biology, The Scripps Research Institute, 10550 North Torrey Pines Rd., La Jolla, California 92037, USA. Phone: 858.784.2728; Fax: 858.784.8166; E-mail: lteyton@scripps.edu (L. Teyton). Phone: 858.784.9706; Fax: 858.784.2980; E-mail: wilson@scripps.edu (I. Wilson).

Kenji Yoshida's present address is: Department of Physiology, Faculty of Pharmacy, Meijo University, Nagoya, Japan.

1. Grumet FC, Coukell A, Bodmer JG, Bodmer WF, McDevitt HO. Histocompatibility (HL-A) antigens associated with systemic lupus erythematosus. A possible genetic predisposition to disease. *N Engl J Med*. 1971;285(4):193–196.
2. Stastny P. Association of the B-cell alloantigen DRw4 with rheumatoid arthritis. *N Engl J Med*. 1978;298(16):869–871.
3. Todd JA, Bell JI, McDevitt HO. HLA-DQ beta gene contributes to susceptibility and resistance to insulin-dependent diabetes mellitus. *Nature*. 1987;329(6140):599–604.
4. Corper AL, et al. A structural framework for deciphering the link between I-Ag7 and autoimmune diabetes. *Science*. 2000;288(5465):505–511.
5. Stratmann T, et al. The I-Ag7 MHC class II molecule linked to murine diabetes is a promiscuous peptide binder. *J Immunol*. 2000;165(6):3214–3225.
6. Latek RR, et al. Structural basis of peptide binding and presentation by the type I diabetes-associated MHC class II molecule of NOD mice. *Immunity*. 2000;12(6):699–710.
7. Yu B, Gauthier L, Hausmann DH, Wucherpfennig KW. Binding of conserved islet peptides by human and murine MHC class II molecules associated with susceptibility to type I diabetes. *Eur J Immunol*. 2000;30(9):2497–2506.
8. Hennecke J, Carfi A, Wiley DC. Structure of a covalently stabilized complex of a human alphabeta T-cell receptor, influenza HA peptide and MHC class II molecule, HLA-DR1. *EMBO J*. 2000;19(21):5611–5624.
9. Reinherz EL, et al. The crystal structure of a T cell receptor in complex with peptide and MHC class II. *Science*. 1999;286(5446):1913–1921.
10. Hovhannisyan Z, et al. The role of HLA-DQ8 beta57 polymorphism in the anti-gluten T-cell response in coeliac disease. *Nature*. 2008;456(7221):534–538.
11. Yoshida K, et al. Evidence for shared recognition of a peptide ligand by a diverse panel of non-obese diabetic mice-derived, islet-specific, diabetogenic T cell clones. *Int Immunol*. 2002;14(12):1439–1447.
12. Stratmann T, et al. Susceptible MHC alleles, not background genes, select an autoimmune T cell reactivity. *J Clin Invest*. 2003;112(6):902–914.
13. Fersht AR. Conformational equilibria in -and -chymotrypsin. The energetics and importance of the salt bridge. *J Mol Biol*. 1972;64(2):497–509.
14. Schreiber G, Fersht AR. Rapid, electrostatically assisted association of proteins. *Nat Struct Biol*. 1996;3(5):427–431.
15. Selzer T, Albeck S, Schreiber G. Rational design of faster associating and tighter binding protein complexes. *Nat Struct Biol*. 2000;7(7):537–541.
16. Shoup D, Szabo A. Role of diffusion in ligand binding to macromolecules and cell-bound receptors. *Biophys J*. 1982;40(1):33–39.
17. Todd JA, et al. Robust associations of four new chromosome regions from genome-wide analyses of type 1 diabetes. *Nat Genet*. 2007;39(7):857–864.
18. Suri A, Walters JJ, Gross ML, Unanue ER. Natural peptides selected by diabetogenic DQ8 and murine I-A(g7) molecules show common sequence specificity. *J Clin Invest*. 2005;115(8):2268–2276.
19. Baker FJ, Lee M, Chien YH, Davis MM. Restricted islet-cell reactive T cell repertoire of early pancreatic islet infiltrates in NOD mice. *Proc Natl Acad Sci U S A*. 2002;99(14):9374–9379.
20. Yang Y, Charlton B, Shimada A, Dal Canto R, Fathman CG. Monoclonal T cells identified in early NOD islet infiltrates. *Immunity*. 1996;4(2):189–194.
21. Kanagawa O, Vaupel BA, Xu G, Unanue ER, Katz JD. Thymic positive selection and peripheral activation of islet antigen-specific T cells: separation of two diabetogenic steps by an I-A(g7) class II MHC beta-chain mutant. *J Immunol*. 1998;161(9):4489–4492.
22. Amrani A, Verdaguer J, Serra P, Tafuro S, Tan R, Santamaria P. Progression of autoimmune diabetes driven by avidity maturation of a T-cell population. *Nature*. 2000;406(6797):739–742.
23. Singer SM, Tisch R, Yang XD, Sytwu HK, Liblau R, McDevitt HO. Prevention of diabetes in NOD mice by a mutated I-Ab transgene. *Diabetes*. 1998;47(10):1570–1577.
24. Zajonc DM, Savage PB, Bendelac A, Wilson IA, Teyton L. Crystal structures of mouse CD1d-iGb3 complex and its cognate Valpha14 T cell receptor suggest a model for dual recognition of foreign and self glycolipids. *J Mol Biol*. 2008;377(4):1104–1116.
25. Garcia KC, et al. Alphabeta T cell receptor interactions with syngeneic and allogeneic ligands: affinity measurements and crystallization. *Proc Natl Acad Sci U S A*. 1997;94(25):13838–13843.
26. Schatz PJ. Use of peptide libraries to map the substrate specificity of a peptide-modifying enzyme: a 13 residue consensus peptide specifies biotinylation in Escherichia coli. *Biotechnology*. 1993;11(10):1138–1143.
27. Vagin A, Teplyakov A. MOLREP: an automated program for molecular replacement. *J Appl Crystallogr*. 1997;30(Pt 6):1022–1025.
28. Brunger AT, et al. Crystallography & NMR system: a new software suite for macromolecular structure determination. *Acta Crystallogr D Biol Crystallogr*. 1998;54(Pt 5):905–921.
29. Emsley P, Cowtan K. Coot: model-building tools for molecular graphics. *Acta Crystallogr D Biol Crystallogr*. 2004;60(Pt 12 Pt 1):2126–2132.
30. Adams PD, et al. PHENIX: building new software for automated crystallographic structure determination. *Acta Crystallogr D Biol Crystallogr*. 2002;58(Pt 11):1948–1954.
31. Laskowski RA, MacArthur MW, Moss DS, Thornton JM. PROCHECK: a program to check the stereochemical quality of protein structures. *J Appl Crystallogr*. 1993;26:283–291.
32. Vriend G. WHAT IF: a molecular modeling and drug design program. *J Mol Graph*. 1990;8(1):52–56, 29.
33. McCoy AJ Grosse-Kunstleve RW, Adams PD Winn MD, Storoni LC Read RJ. Phaser crystallographic software. *J Appl Crystallogr*. 2007;40(Pt 4):658–674.